Electron-impact excitation of open d-shell ions

Published in:
Journal of Physics: Conference Series

Document Version:
Publisher's PDF, also known as Version of record

Queen's University Belfast - Research Portal:
Link to publication record in Queen's University Belfast Research Portal

Electron-impact excitation of open d-shell ions.

C A Ramsbottom, C P Ballance, A Hibbert and F P Keenan.

School of Mathematics & Physics, Queen's University Belfast, Befast BT7 1NN, Northern Ireland.

E-mail: `c.ramsbottom@qub.ac.uk`

Abstract.   Astrophysics is driven by observations, and in the present era there are a wealth of state-of-the-art ground-based and satellite facilities. The astrophysical spectra emerging from these are of exceptional quality and quantity and cover a broad wavelength range. To meaningfully interpret these spectra, astronomers employ highly complex modelling codes to simulate the astrophysical observations. Important input to these codes include atomic data such as excitation rates, photoionization cross sections, oscillator strengths, transition probabilities and energy levels/line wavelengths. Due to the relatively low temperatures associated with many astrophysical plasmas, the accurate determination of electron-impact excitation rates in the low energy region is essential in generating a reliable spectral synthesis. Hence it is these atomic data, and the main computational methods used to evaluate them, which we focus on in this publication. We consider in particular the complicated open d-shell structures of the Fe-peak ions in low ionization stages. While some of these data can be obtained experimentally, they are usually of insufficient accuracy or limited to a small number of transitions.

1. Introduction

The accurate determination of electron-impact excitation rates for ions of the Fe-peak elements remains a challenge at the forefront of atomic collision physics. These atomic data, particularly for the low-ionization stages of Fe, Ni and Co, are of crucial importance in the quantitative analysis of many astronomical spectra and can provide the key to our understanding of the early Universe and star formation. A wealth of observations of these species in low-ionization stages have been found to dominate the spectra of astronomical sources as diverse as the Sun and other stars, gaseous nebulae, active galactic nuclei, quasars and supernovae remnants. For example [1] presented a detailed study of the symbiotic star AG Pegasi in the ultraviolet wavelength region and of the 600 lines observed in the spectra from IUE, HST and FUSE, 346 were identified as Fe II emission lines. In addition emission lines of singly ionised nickel (Ni II), the heaviest and second most abundant Fe-peak element, are frequently observed in nebular spectroscopy. An example is found in the STIS observations of the Strontium Filament in Eta Carinae where a wealth of emission lines of Ni II were observed [2].

However, difficulties arise in the calculation of the collision cross sections for these ions, due to the complexity of the open d-shell target which gives rise to many hundreds of target states for each electronic configuration and typically thousands of closely coupled channels. Hence these target states require large configuration interaction expansions for their accurate representation. These ions are particularly difficult since they involve transitions of the type $3d^n \rightarrow 3d^{n-1}4s,4p,4d$. To illustrate these difficulties, we present in Figure 1 the energy level diagram

of Fe II below 30,000 cm^{-1} ($\approx$ 3.72 eV) taken from the tables of [3] and [4], indicating some of the forbidden infrared and optical transitions observed in gaseous nebulae. Clearly visible in this low energy region are the 16 LS-coupled terms and the resulting 46 fine-structure levels. In addition many more higher-lying terms will play a significant role in the determination of the excitation cross sections, acting as virtually excited intermediate states. To compound these computational difficulties, the low-energy electron scattering region is dominated by an infinite number of Rydberg resonances converging on to each target state threshold. A very fine mesh of incident electron energies is required to resolve these narrow structures, typically involving many ten of thousands of individual energy points.
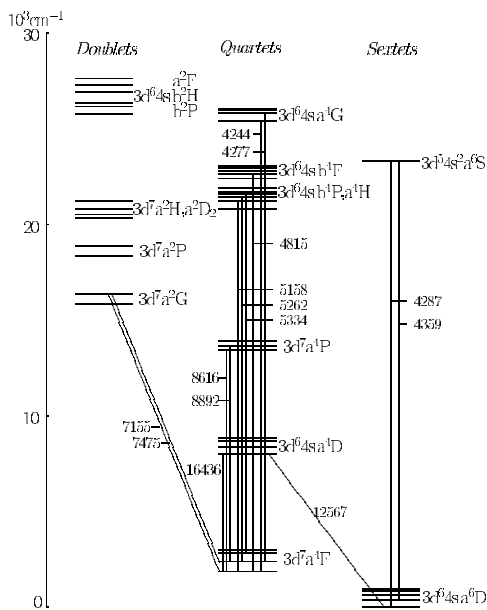

Figure 1. The 16LS terms of Fe II below 30,000cm^{-1} showing the corresponding 46 fine-structure levels and some forbidden and optical lines observed in gaseous nebulae with their wavelengths in Å.

Many computer packages have been developed over the years to compute collisional and radiative data for atoms and ions, the R-matrix method being one of the more powerful and reliable. For the Fe-peak ions the computational effort required is extensive and well beyond serial electron collision programs. New parallel variants of the R-matrix codes have been developed, BP RMATRXI, DARC, RMATRXII + FINE, BSR and ICFT, which are now capable of exploiting HPC facilities, making these calculations currently feasible. Comparing the atomic data for a selection of Fe-peak ions evaluated using these differing variants of the R-matrix codes is the focus of this paper.

2. The R-Matrix Method
R-matrix theory is based on the partitioning of space into two regions, internal and external, which depend on the radial distance r of the scattered electron from the target nucleus. The solution in each region is determined independently and the R-matrix then links the solutions on the boundary $r = a$ of these regions.

Computer packages describing the R-matrix approach have a long history, with the first publication dating back to 1974. This LS-coupled version (RMATRX I) published by [5] was based on the theory developed by [6], [7] and [8], and the original codes were modified by [9]. These particular packages were appropriate for use with light atoms and ions, where relativistic effects could be neglected and the (N+1)-electron Hamiltonian (in a.u.) was defined by

$$H^{N+1} = \sum_{i=1}^{N+1} \left(-\frac{1}{2}\nabla_i^2 - \frac{Z}{r_i} + \sum_{i>j=1}^{N+1} \frac{1}{r_{ij}} \right) \tag{1}$$

where $\mathbf{r_i}$ is the vector co-ordinate of the *ith* electron and $r_{ij} = |\mathbf{r_i} - \mathbf{r_j}|$ is an inter-electronic distance. As the nuclear charge Z increases, however, relativistic effects both in the target wavefunction and in the wavefunction representing the scattered electron become important even at low scattering energies. Hence the Breit-Pauli Hamiltonian given by

$$H_{BP}^{N+1} = H^{N+1} + H_{REL}^{N+1} \tag{2}$$

needs to be adopted. Only the one-electron relativistic terms, the mass-correction, the one-electron Darwin and the spin-orbit, are explicitly retained resulting from the reduction of the Dirac equation to the Breit-Pauli form. Hence the low-Z Breit-Pauli Hamiltonian for an (N+1)-electron system is taken to be

$$H_{BP}^{N+1} = H^{N+1} + H_{Mass}^{N+1} + H_{D_1}^{N+1} + H_{SO}^{N+1} \tag{3}$$

The first publication of the Breit-Pauli version of the R-matrix computer packages (BP) by [10] has since been modified by [11]. Parallel variants of both RMATRX I and BP RMATRX I are also available, see [12]. For heavy atoms and ions where the nuclear charge Z is large, relativistic effects must be included via the Dirac Hamiltonian:

$$H_D^{N+1} = \sum_{i=1}^{N+1} \left(c\alpha.\mathbf{p}_i + \beta'c^2 - \frac{Z}{r_i} \right) + \sum_{i>j=1}^{N+1} \frac{1}{r_{ij}} \tag{4}$$

where α and $\beta' = \beta - I_4$ are 4×4 dimensional Dirac matrices defined by

$$\alpha = \left(\begin{array}{cc} 0 & \sigma \\ \sigma & 0 \end{array} \right) \qquad \beta = \left(\begin{array}{cc} I_2 & 0 \\ 0 & -I_2 \end{array} \right)$$

where the components of σ, σ_x, σ_y and σ_z are 2×2 Pauli spin matrices given by

$$\sigma_x = \left(\begin{array}{cc} 0 & 1 \\ 1 & 0 \end{array} \right) \qquad \sigma_y = \left(\begin{array}{cc} 0 & -i \\ i & 0 \end{array} \right) \qquad \sigma_z = \left(\begin{array}{cc} 1 & 0 \\ 0 & -1 \end{array} \right)$$

and I_2 and I_4 are 2×2 and 4×4 unit matrices, respectively. A fully relativistic R-matrix collision program DARC was developed by [13] to study electron collisions with heavy atoms and ions. Since that time many extensions and modifications have been made to the original DARC codes. These include the parallelisation of the integral generation, the Hamiltonian formation and diagonalization [12]. All of the codes mentioned above have been used extensively to study electron and photon-collisions with atoms and ions for nearly four decades, and have been tested against each other for different systems and processes, and are well established computer packages in the field. For example, the DARC and BP codes have previously been tested against each other for Fe $^{14+}$ [14], where it was conclusively shown that the resulting effective collision strengths varied between the two approaches at the 5% level.

However, one difficulty arises when using the Breit-Pauli or Dirac Hamiltonian rather than the non-relativistic one. The difficulty is computational and arises from the fact that the number of coupled channels is greatly increased for the same ionic model when a relativistic expansion, rather than a non-relativistic expansion, is adopted in the internal region. A sample case is shown in Table 1 for Fe II where it can clearly be seen that as the model increases in sophistication with the addition of more and more target level configurations, the number of fine-structure states, and more importantly the number of coupled channels involved, increases dramatically beyond computational capacity. The same cannot be said if we remain in the LS-coupling scheme for a comparative model. In addition, the size of the Hamiltonian matrices that need to be

Table 1. Fe II model growth in LSπ and Jπ couplings.

Model	LSπ		Jπ	
	States	Channels	States	Channels
1 config $3d^6 4s$	24	72	63	420
2 config $3d^7$	32	98	82	540
3 config $3d^6 4p$	100	315	262	1800
4 config $3d^5 4s^2$	116	363	299	2052
5 config $3d^5 4s4p$	261	805	716	5076
6 config $3d^6 5s$	285	877	779	5496
7 config $3d^6 4d$	389	1239	1055	7596

Table 2. Hamiltonian size and channel growth for several Fe II models .

No. Target States	Max No. Channels	Max size of (N+1) H matrix	Total No. Transitions
100 (LSπ)	315	12660	5050
262 (Jπ)	1800	36055	34453
716 (Jπ)	5076	> 100 000	256 686

diagonalized increase significantly. This can be seen in Table 2 for a sample of the Fe II models listed in Table 1. Clearly the collision calculation becomes computationally more dependant and in some cases impossible to complete. To address these issues a number of frame-transformation methods have been developed which omit the relativistic terms in the Hamiltonian in the internal region but ensure that they are included in the external and asymptotic regions. One such procedure is the intermediate-coupling frame transformation (ICFT) method of [15] where multi-channel quantum defect theory (MQDT) is employed to generate LS-coupled 'unphysical' K-matrices on the boundary of the asymptotic region. These matrices are then transformed initially to jK coupling and finally to full intermediate coupling using term-coupling coefficients. The physical K-matrices are then obtained from their unphysical counterparts in intermediate coupling using MQDT. This transformation method has been widely used and tested against the Breit-Pauli R-matrix approximation, see for example calculations of electron-impact excitation for Fe^{14+} performed by [15] where an excellent level of agreement between the two methods was found.

In 1994, [16] developed a new parallel suite of computer packages, RMATRX II, implementing R-matrix theory in the internal region with the specific goal of reducing time-consuming operations enabling complex open d-shell Fe-peak systems to be attempted. The diagonalized Hamiltonian matrices are computed in the internal region using LS coupling. Relativistic effects are then incorporated via a frame-transformation method using the computer package FINE [17]. Unlike the ICFT procedure discussed above, this method transforms the R-matrices in LSπ coupling at energy E into R-matrices in Jπ pair coupling, and the transformation is carried out earlier on the R-matrix partitioning the internal and external regions. In addition, in this new transformation procedure it is the energy independent surface amplitudes that are transformed so that the recoupling is performed only once for each LSπ and Jπ symmetry rather than for

each scattering energy E. Similar to the ICFT method, the term splitting in the target is taken into account via the term-coupling coefficients. These new packages RMATRX II + FINE have been employed to compute collision strengths for the electron-impact excitation of complex open d-shell Fe-peak ions such as Ni II [18], Cr II [19] and Sc II [20]. However, they have never been rigorously compared to the well established relativistic BP and DARC codes for a full collision calculation; only simple test evaluations have been performed for simple models. This is the purpose of the present publication.

A final package which exists for the calculation of electron-impact collision strengths is the B-spline R-matrix (BSR) suite of codes developed by [21]. In BSR the Breit-Pauli Hamiltonian is used and in DBSR the fully relativistic Dirac Hamiltonian is adopted instead. The main difference between BSR and the previously mentioned R-matrix codes concerns the orthogonality of the target orbitals. The BP RMATRX I, RMATRX II + FINE, DARC and ICFT all use an orthogonal orbital basis. There is, however, no physical need for the orbitals to be orthogonal. In BSR the continuum basis is described by B-splines allowing for the use of non-orthogonal orbitals. It should be noted that all the R-matrix variants discussed above marry with the STGF external region code originally developed by Seaton (unpublished).

3. Results and Discussion

In this section we provide an in-depth comparison of collision strengths and effective collision strengths produced using all variants of the R-matrix codes. We consider a selection of ions focussing on the important Fe-peak species. The collision strength between an initial state i and a final state j, $\Omega(i, j)$, is defined in terms of the collision cross section by

$$\Omega(i, j) = \frac{(2J_i + 1)k_i^2}{\pi}\sigma(j \to i). \tag{5}$$

Of particular importance in astrophysical and laboratory plasma applications are the corresponding effective collision strengths. These Υ_{ij} are obtained by averaging the delineated collision strengths over a Maxwellian distribution of electron velocities so that

$$\Upsilon_{ij}(T_e) = \int_0^\infty \Omega_{ij}(E_f) \exp(-E_f/kT_e)d(E_f/kT_e) \tag{6}$$

where T is the electron temperature in Kelvin, k is Boltzmann's constant and E_f is the final kinetic energy of the electron.

We begin with the electron-impact excitation of the Fe-peak Cr II ion which was subjected to an extensive RMATRX II + FINE transformation evaluation by [19]. A total of 108LS/280jj target levels formed from the $3d^5$, $3d^4 4s$ and $3d^4 4p$ basis configurations were included in the wavefunction expansion, including all doublet, quartet and sextet terms. These states were represented by configuration-interaction type wavefunction expansions in terms of nine orthogonal basis orbitals, 1s, 2s, 2p, 3s, 3p, 3d, 4s, 4p and $\overline{4d}$. Configuration interaction and correlation effects were carefully considered by the inclusion of seven more configurations, namely $3d^3 4s^2$, $3d^3 4p^2$, $3d^3 3s3p$, $3d^4 4d$, $3d^3 4s4d$, $3d^3 4p4d$ and $3d^3 4d^2$. As stated earlier, one of the advantages of working with the non-relativistic Hamiltonian in the internal region is to keep the calculation to a manageable level. Reducing the number of coupled channels, and in turn the size of the Hamiltonian matrices that need to be diagonalized, keeps the evaluations tractable. To perform the comparison this model has been incorporated into the Breit-Pauli codes and the evaluations undertaken on the US HPC facilities at NERSC. We present in Figure 2 the collision strength as a function of incident electron energy in Rydbergs for the lowest-lying transition from the ground $3d^5$ $^6S_{5/2}^e$ to the first excited $3d^4 4s$ $^6D_{1/2}^e$ level. Clearly there is excellent agreement between the results produced by the Breit-Pauli and the RMATRX II + FINE frame-transformation methods. The resonance profiles are identical and the background cross sections

compare exceptionally well. In Figure 3 we present the Maxwellian averaged effective collision strengths for the five lowest-lying transitions $3d^5$ $^6S^e_{5/2}$ - $3d^44s$ $^6D^e_{1/2,3/2,5/2,7/2,9/2}$ plotted as a function of astrophysically relevant temperatures in Kelvin. As expected, excellent agreement between the two methods is found for all transitions and for all temperatures. In conclusion, it is apparent that the RMATRX II plus FINE transformation approach to electron-impact excitation of Cr II produces atomic data of a similar quality to a full Breit-Pauli treatment.   In Figures 4
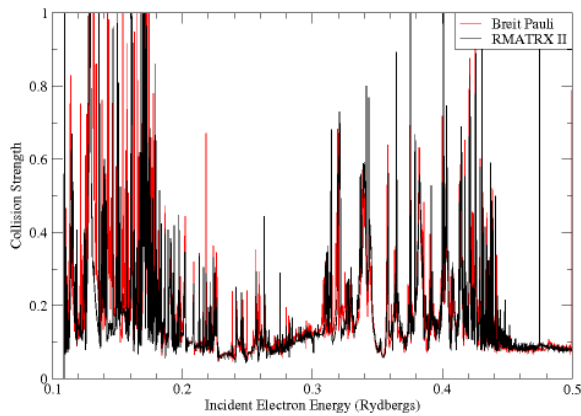
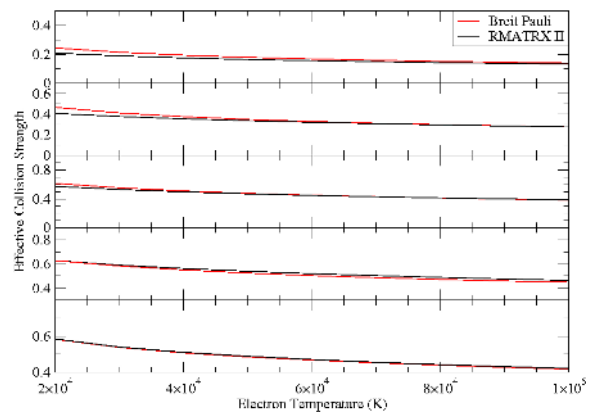**Figure 2.** Cr II collision strength for $3d^5$ $^6S_{5/2}$ - $3d^44s$ $^6D_{1/2}$ transition.

Figure 3. Cr II effective collision strengths for $3d^5$ $^6S_{5/2}$ - $3d^44s$ $^6D_{1/2,3/2,5/2,7/2,9/2}$.
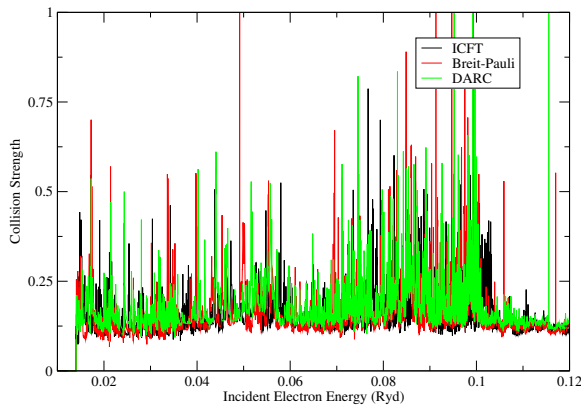

Figure 4. Mn V collision strength for $3d^3$ $^4F_{3/2}$ - $3d^3$ $^2D2_{5/2}$ transition.
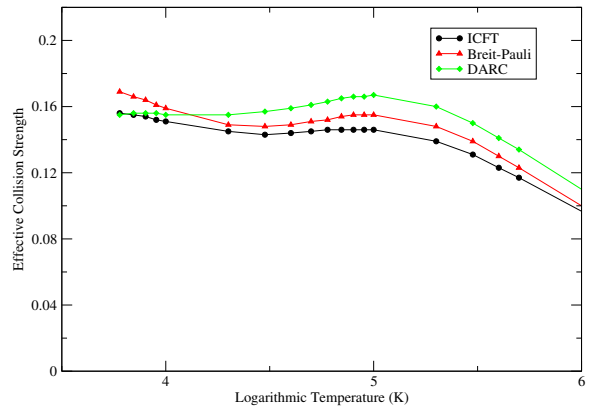

Figure 5. Mn V effective collision strength for $3d^3$ $^4F_{3/2}$ - $3d^3$ $^2D2_{5/2}$ transition.

and 5 we consider a more highly ionized Fe-peak element, Mn V, with ground state configuration $3d^3$ $^4F_{3/2}$ [22]. The target model incorporated the lowest 80 fine-structure levels arising from the $3d^3$, $3d^24s$ and $3d^24p$ configurations. Collision strengths and effective collision strengths were computed using the BP RMATRX I, ICFT transformation and fully relativistic DARC codes. We compare in Figure 4 the collision strengths as a function of incident electron energy in Ryds for the spin forbidden $3d^3$ $^4F_{3/2}$ - $3d^3$ $^2D2_{5/2}$ transition. The corresponding effective collision strengths are shown in Figure 5 plotted as a function of log electron temperature in Kelvin. Clearly the three data sets are within 10% of each other indicating that for this forbidden line, all three methods produce atomic data of a similar level of accuracy. Discrepancies for all other transitions considered were found to be comparable.
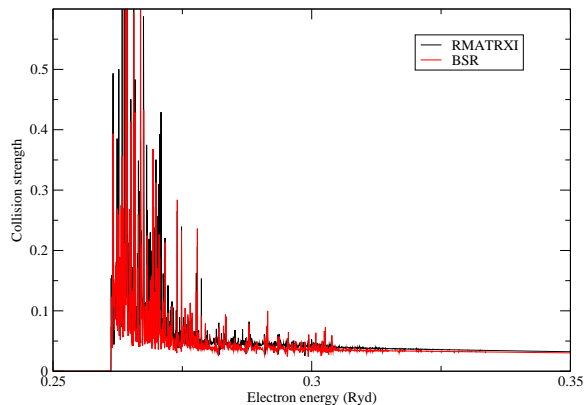
Figure 6. Mg VIII collision strength for $2s^2 2p$ $^2P^o_{1/2}$ - $2p^3$ $^2P^o_{3/2}$ transition.
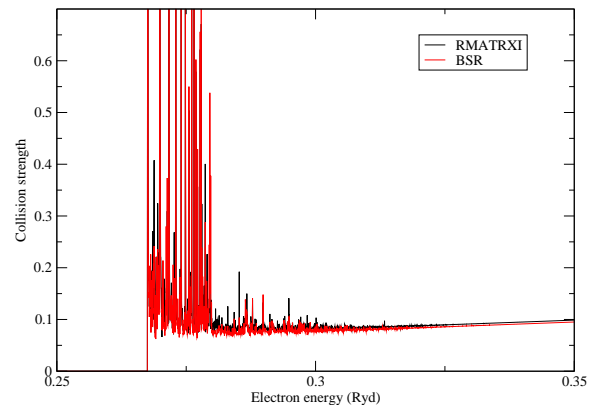

Figure 7. Mg VIII collision strength for $2s^2 2p$ $^2P^o_{1/2}$ - $2p^3$ $^2D_{3/2}$ transition.

Finally in Figures 6 and 7 we present data for a 125 fine-structure level calculation for Mg VIII [23]. The collision strengths were determined using the BP RMATRX I codes, but also in jK coupling with the BSR codes for the first few partial waves. High levels of agreement were again found for the two transitions displayed, the $2s^2 2p$ $^2P^o_{1/2}$ - $2p^3$ $^2P^o_{3/2}$ and the $2s^2 2p$ $^2P^o_{1/2}$ - $2p^3$ $^2D_{3/2}$ transitions. In summary, all the results presented above indicate that it is unimportant which variant of the R-matrix codes that are adopted in the evaluation of the atomic data. Relativistic and LS transformed models all produce rates of a similar accuracy.

The Fe-peak ion Fe II is particularly important for astrophysical applications due to its high cosmic abundance. Very few objects exist in any class of astronomy which do not show large numbers of emission and/or absorption lines of Fe II in their spectrum from the infrared to ultraviolet wavelengths. Despite its importance, little agreement has been found among the various theoretical predictions currently available, particularly for low-lying fine-structure transitions. In Figures 8 and 9 we present a complete representation of all the effective collision strength data currently available for the two lowest-lying forbidden transitions in Fe II, $3d^6 4s$ $^6D_{9/2}$ - $3d^6 4s$ $^6D_{7/2}$ and $3d^6 4s$ $^6D_{9/2}$ - $3d^6 4s$ $^6D_{5/2}$. Displayed in the figures are the 262 level model of [24] (corresponding to the model outlined in row 2 of Table 2), the 142 level model of [25], earlier work of [26] and [27] and the extrapolated data of [28]. We see that even at 10^4 K, the temperature at which Fe II is most frequently observed, little agreement is found with discrepancies of up to 50% noted between highest and lowest values.

Another issue arises due to the size of these models with the largest (262-level) described by [24] including explicit target levels up to an energy of approximately 10.85 eV. A recent paper by [29] reported the observation and analysis of the unusually luminous, narrow-line quasar PHL 1811. It was found that the near UV-spectrum was dominated by very strong Fe II lines but it was also inferred that Fe II emission was observed from levels as highly excited as 14eV. Since these luminous quasars are probes of the early Universe it is important that all astrophysical models of Fe II are improved and extended to successfully complete this significant application. We have initiated the largest systematic study of the electron-impact excitation of Fe II with a model incorporating 716 fine-structure levels formed from the five basis configurations $3d^6 4s$, $3d^7$, $3d^5 4s^2$, $3d^6 4p$ and $3d^5 4s4p$, corresponding to 5076 coupled channels and 255,970 individual transitions. This model thus includes explicit target levels that extend up to approximately 23eV, highly relevant to the astrohphysical applications discussed above. Results from this extensive calculation will be discussed at the conference.
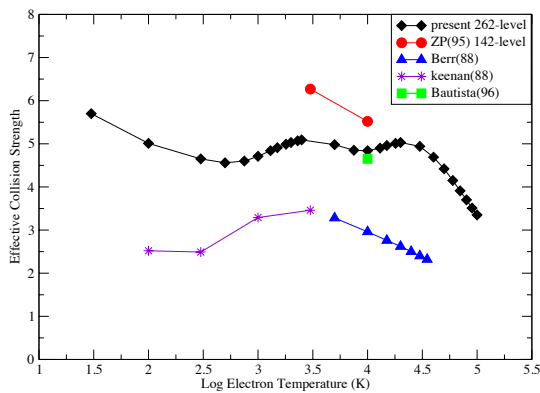
Figure 8. Fe II effective collision strengths for $3d^6 4s\ ^6D_{9/2}$ - $3d^6 4s\ ^6D_{7/2}$ transition.
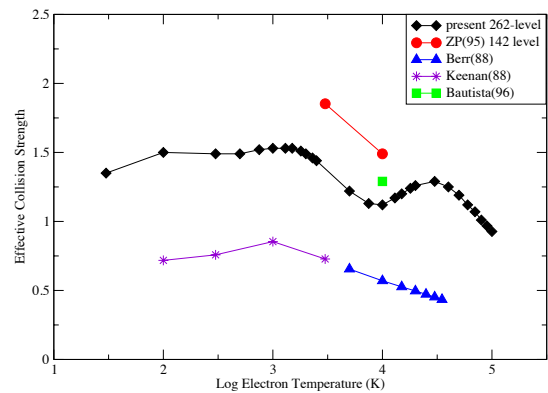

Figure 9. Fe II effective collision strengths for $3d^6 4s\ ^6D_{9/2}$ - $3d^6 4s\ ^6D_{5/2}$ transition.

4. Acknowledgements

5. References

[1] Eriksson M, Johansson S & Wahlgren G M, 2006, A&A, 451, 157
[2] Hartman H. Gull T, Johansson S & Smith N. 2004, HST Eta Carinae Treasury Project Team, A&A, 419, 215
[3] Johansson S, 1978, Phys.Scr., 18, 217
[4] Corliss C & Sugar J, 1982, J.Phys.Chem.Ref.Data, 11, 135
[5] Berrington KA, Burke PG, Chang JJ, Chivers AT, Robb WD & Taylor KT, 1974, Comp.Phys.Comm., 8, 149
[6] Burke PG & Seaton MJ, 1971, Methods Comp.Phys., 10, 1
[7] Burke PG, Hibbert A & Robb WD, 1971, J.Phys.B:At.Mol.Phys, 4, 153
[8] Burke PG & Robb WD, 1975, Adv.At.Mol.Phys., 11, 143
[9] Berrington KA, Burke PG, LeDourneuf M, Robb WD, Taylor KT & Lan VK, 1978, Comp.Phys.Comm.,14,367
[10] Scott NS & Taylor KT, 1982, Comp.Phys.Comm., 25, 347
[11] Berrington KA, Eissner W & Norrington PH, 1995, Comp.Phys.Comm., 92, 290
[12] Ballance CP & Griffin DC, 2004, J.Phys.B:At.Mol.Opt.Phys., 37, 2943
[13] Norrington PH & Grant IP, 1987, J.Phys.B:At.Mol.Opt.Phys., 20, 4869
[14] Berrington KA, Ballance CP, Griffin DC & Badnell NR, 2005, J.Phys.B.At.Mol.Opt.Phys., 38, 1667
[15] Griffin DC, Badnell NR & Pindzola MS, 1998, J.Phys.B:At.Mol.Opt.Phys., 31, 3713
[16] Burke PG, Burke VM & Dunseath KM, 1994, J.Phys.B:At.Mol.Opt.Phys., 27, 5341
[17] Burke VM, *private communication*
[18] Cassidy CM, Ramsbottom CA & Scott MP, 2010, a&A, 513, A55
[19] Wasson IR, Ramsbottom CA & Scott MP, 2010, A&A, 524, A35
[20] Grieve MFR & Ramsbottom CA, 2012, MNRAS, 424, 2461
[21] Zatsarinny O, 2006, Comp.Phys.Comm., 174, 273
[22] Grieve MFR, Ramsbottom CA, Hibbert A, Ferland G & Keenan FP, 2015, *in preparation*
[23] Grieve MFR, Ramsbottom CA & Keenan FP, 2013, A&A, 556, A24
[24] Ramsbottom CA, Hudson CE, Norrington PH & Scott MP, 2007, A&A, 475, 765
[25] Zhang HL & Pradhan AK, 1995, A&A, 293, 953
[26] Berrington KA, Burke PG, Hibbert A, Mohan M & Baluja KL, 1988, J.Phys.B., 21, 339
[27] Bautista MA & Pradhan AK, 1996, A&AS, 115,551
[28] Keenan FP, Hibbert A, Burke PG & Berrington KA, 1988, ApJ, 332, 539
[29] Leighly KM, Halpern JP, Jenkins EB & Casebeer D, 2007, ApJSS, 173, 36